applied mechanics

Article

Crack Growth Analysis of a Welded Centre Sill in a Hopper Wagon

Daren Peng [1,2,*], Rhys Jones [1,2] and Andrew S. M. Ang [2]

[1] Centre of Expertise in Structural Mechanics, Department of Mechanical and Aeronautical Engineering, Monash University, Wellington Rd, Clayton, VIC 3800, Australia; rhys.jones@monash.edu
[2] ARC Training Centre in Surface Engineering for Advanced Materials (SEAM), Swinburne University of Technology, H38, P.O. Box 218, Hawthorn, VIC 3122, Australia; aang@swin.edu.au
* Correspondence: daren.peng@monash.edu

Abstract: This paper mainly studies the fatigue cracks growth of fillet weld specimens in a fashion that is consistent with that used to assess the fatigue performance of complex aerospace structures under operational flight loads. The fatigue test loads were determined using the overall finite element analysis results of the hopper wagon. The actual applied test loads were monitored using strain gauges. The residual stress in the critical region was determined by combining the stress field of the welded specimen obtained by a thermal imager under cyclic loading with the results of the three-dimensional finite element analysis of the specimen. During the fatigue test, a digital camera (with microscope lens) was used in conjunction with infrared measurement technology to obtain the crack growth information. As in prior studies, the three dimensional finite element alternating technique was used to calculate the stress intensity factor in the critical area of the crack in the fillet weld specimen. The Hartman–Schijve crack growth equation was then used, in conjunction with the calculated stress intensity factor solutions, to compute the crack growth history in a fatigue test of a critical welded component in a hopper wagon. The resultant computed crack growth histories are relatively consistent with the test results.

Keywords: hopper wagon; infrared measurement; finite element method

Citation: Peng, D.; Jones, R.; Ang, A.S.M. Crack Growth Analysis of a Welded Centre Sill in a Hopper Wagon. *Appl. Mech.* **2024**, *5*, 762–772. https://doi.org/10.3390/applmech5040042

Received: 29 August 2024
Revised: 7 October 2024
Accepted: 12 October 2024
Published: 25 October 2024

1. Introduction

Fabrication by welding is very popular in the railway industry due to its effectiveness in reducing production costs. Hopper wagons are railway freight cars used to transport a variety of materials such as ore, coal, ballast, bulk cargo and minerals, as well as grain [1,2]. As a hopper wagon is a complex structure composed of multiple steel components welded together, the region near the weld toe is often prone to fatigue failure due to residual stresses and stress concentration. In fact, cracks usually initiate at the toe of the weld that connects the centre sill to another part of the car body [3]. Therefore, this is an important safety issue that the railway industry must take seriously. In particular, the ability to accurately predict the time for a small non-detectable flaw to reach failure size is important.

In the published literature, no reports on the fatigue life analysis of hopper wagons were found. An engineering approach to the fracture assessment of hopper wagons was provided in [3]. This approach was an engineering method based on the energy method for calculating the two-dimensional (2D) stress intensity factor of the cracks at the centre sill. Since the hopper car can be considered as a thin-walled structure, the cracks in the centre sill can be assumed to be akin to two-dimensional cracks. The approach presented in [3] did not involve any crack growth analysis issues. Some studies on the fatigue strength of other types of wagons were found [4–8]. One can also refer to relevant technical specifications for fatigue strength assessment [9–11]. However, all these studies/approaches were based on the S-N method (stress–life curve method). This paper proposes a new method, which employs the concept of damage tolerance analysis, to study the crack growth of the welded

centre sill in a hopper wagon. Damage tolerance is a relatively new structural fatigue analysis theory. It mainly adopts the fracture mechanics analysis method; that is, by analysing the change process of the stress intensity factor and other parameters with cyclic loads in the presence of defects/cracks, it ensures that these parameters are not greater than the critical value (fracture toughness) during the effective life or maintenance cycle.

The approach provided in this paper includes the following parts. First of all, test specimens were made by cutting the material from the parts where cracks were found (toes of the welds connecting the centre sill). A three-dimensional (3D) finite element model [12] (without considering cracks) was built to obtain the stresses of the hopper wagon, in order to determine the loads applied to the specimen during crack growth testing. Second, a CEDIP (Paris, France) JADE® medium-wave infrared camera was used to measure the stress field, combining it with a 3D finite element solution to obtain residual stress at the toe region of the welded specimen undergoing cyclic loading (as the residual stress in the welded specimen could have an effect on the crack growth in a welded specimen). Both the infrared camera system and a digital camera were used to monitor the crack growth from the initiation of the crack to the failure of the specimen. A pair of strain gauges were used to validate the infrared measurement and 3D finite element model. In the third part, the crack growth analysis and the comparison with the experimental results were completed. The stress intensity factor needs to be calculated before performing the crack growth analysis. The actual centre sill has a certain thickness (such as 9 mm), and the cracks usually initiates from the surface of the weld toe. The fatigue life required for a crack to penetrate the thickness from its initial state accounts for the vast majority of the total life of the centre sill. It is very meaningful to study the growth of surface cracks in the centre sill. The method provided by [3] is only suitable for dealing with the fracture strength problems of two-dimensional cracks and cannot be used to calculate the stress intensity factors of surface cracks. Therefore, in order to complete the task proposed in this section, a semi-analytical method [13,14] was used to calculate the stress intensity factors of the surface cracks in the fillet welded specimen at the critical region. The resultant stress intensity factor solution is then used in conjunction with the Hartman-Schijve crack growth Equation [15–18] to calculate the increment in the crack growth per cycle.

The method used to calculate the stress intensity factor solution around the crack front is based on the three-dimensional finite element alternating technique outlined in [19–23], which is a semi-analytical algorithm that involves the use of an analytical solution combined with a numerical technique to obtain the stress intensity factors. Here it should be noted that, the Hartman–Schijve crack growth equation [24] is extensively used in the open literature to predict crack growth [15–18,25–30].

Since the alternating finite element method is used to calculate stress intensity factors, it is not necessary to consider the existence of actual cracks in the finite element model, and only the stress distribution in the crack surface need be obtained using an ordinary finite element method. Therefore, one can greatly avoid the need for fine meshes at the crack tip when modelling the cracks. Only coarser meshes need to be used, thereby shortening the analysis time. As such, this paper extends the methodology used in [15,30,31] to assess the durability of aerospace structures to welds in rail structures. This method also has great advantages in predicting crack growth in complex structures such as a hopper wagon, etc.

2. Test Loads Determination Methodology

First, the distribution of the stress in the surface of the crack must be known. As the crack is not modelled explicitly, an uncracked finite element model is needed to obtain the stress distribution of the location for crack development within a member known as the centre sill. A finite element model of the hopper wagon was developed using the finite element pre and post processor FEMAP software program [12]. Due to symmetry, only one quarter of the hopper wagon needed to be modelled. The resultant mesh and the maximum principal stress contour are provided in Figure 1. Usually, hopper cars are subjected to the combined effects of traction load, live load + static load, buffer load, etc. Compared with

the traction load, the local stress caused by the live load + static load and buffer load in the area where the crack occurs in the middle beam is very small. Therefore, the stresses introduced by draft loading (1560 kN) have been considered in this paper. It is worth noting that the 1560 kN here refers to the maximum value in the measured (operational) load spectrum. A material density of 7850 kg m^3 was used for all materials. Here, the thickness of the plate containing the fatigue cracks region was 9 mm. The centre sill was made of mild steel, the Young's modulus (E) and Poisson's ratio (μ) being 200,000 MPa and 0.3 respectively. The finite element models included approximately 92,914 CQUAD4 (Quadrilateral Plate Element Connection, see [12]) elements and 91,294 nodes.

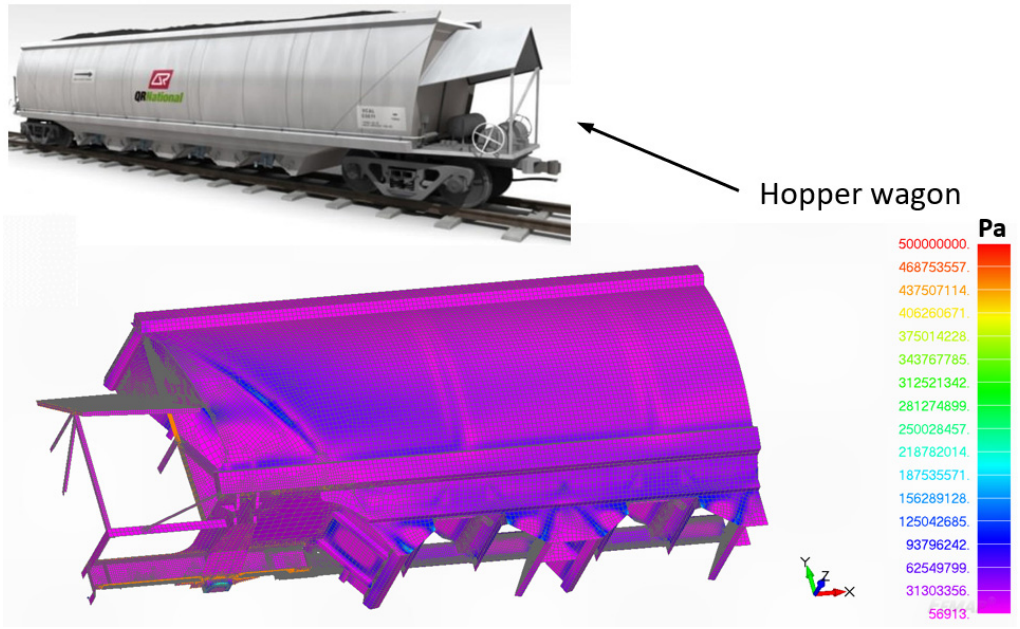

Figure 1. The resultant mesh and maximum principal stress contour for the hopper wagon. The stress units are in Pa.

Figure 2 shows the local maximum principal stress contour in the crack-initiated region of the centre sill under draft loading. At the crack location (Figure 2), the element size was 1.072 mm. The calculated maximum principal stresses were 497 MPa and 253.9 MPa in the toe and non-stress concentration area (36 mm from the toe root was selected in this paper, and a detailed explanation of why 36 mm was chosen is provided in Section 3). The above results can be used to determine the load required for the test. Figure 3 shows a test specimen made from a portion of the structure cut near the critical area.

When the stresses at the toe and non-stress concentration area of the specimen during the fatigue test are close to the calculation results of the finite element of the hopper wagon, the loads applied to the fatigue machine are the "test loads". For convenience, a finite element analysis can be performed on the specimen. The applied loads of the finite element model can be repeatedly adjusted until the stresses calculated at the toe and non-stress concentration area are consistent with (or close to) the calculation results obtained from the finite element of the hopper wagon. The corresponding loads will be the test loads. Before the fatigue test, it is necessary to use resistance strain to measure the strain in the region of the non-stress concentration area and use infrared to detect the stress distribution in the both the toe and non-stress concentration area to ensure the correctness of the applied test loads.

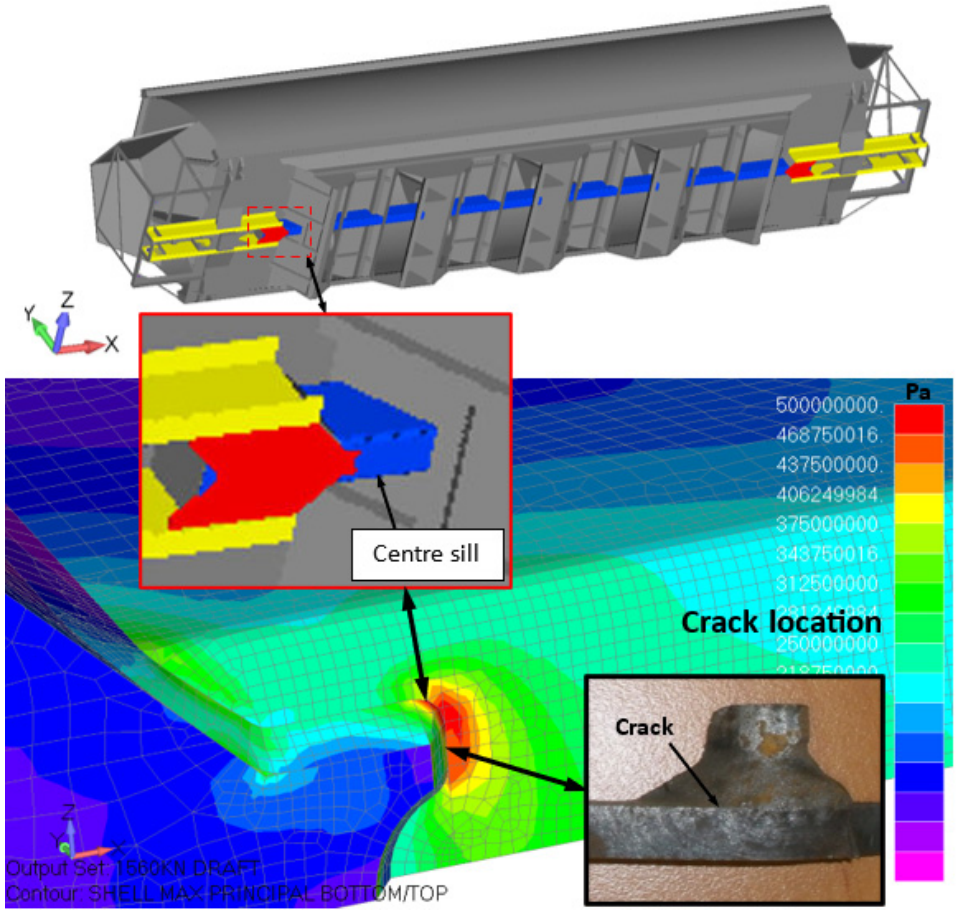

Figure 2. The local maximum principal stress contour in the crack-initiated region of the centre sill under draft loading. The stress units are in Pa.

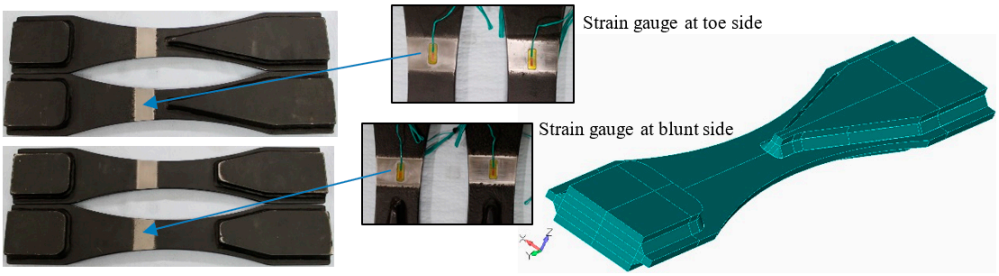

Figure 3. Test specimen and geometry of FEM model.

3. Test Process and Results

The steel test specimen was cut from the centre sill of a hopper wagon; see Figure 3. Each welded specimen was fitted with two strain gauges to monitor the stress during the test. These two strain gauges were positioned on the welded toe and blunt side surfaces at a location of 36 mm from the welded toe corner (equal to 4× the material thickness). Saint-Venant's principle was used to avoid stress concentrations; see Figure 4. The strain gauges used in this test were SHOWA (Tokyo, Japan) N11-FA-5-120-11-W strain gauges, each having the following parameters:

Gauge length:	5 mm;
Resistance:	120 ± 0.3%;
Gauge factor:	2.05 ± 1%;
Temp Comp for Steel:	11;
Thermal Output:	±2 microstrain/°C.

The measuring and recording equipment used for this test consisted of

- National Instruments (Macquarie Park, NSW, Australia) NI SCXI–1000 Chassis;
- National Instruments NI SCXI–1520 8-Channel Universal Strain/Bridge;
- National Instruments NI SCXI–1100 32-Channel Multiplexer Amplifier;
- National Instruments NI SCXI–1314 Module;
- National Instruments DAQCard–6036E (Austin, TX, USA), 16 Inputs/2 Outputs, 200 kS/s, 16-bit Multifunction I/O Data Acquisition Card.

The specimen was fatigue tested at a frequency of 5~10 Hz in an MTS 500 facility, and the applied loading was axial tension. The cyclic loading was taken to a range of 5 to 75 KN with a frequency of 5 Hz. The setup is shown in Figures 5 and 6. The cyclic loading range corresponded to the largest cycle in a measured (operational) load spectrum. This is of course a more conservative approach. A 5 Hz frequency was selected to avoid overheating the specimen during the test and thus affecting the test results.

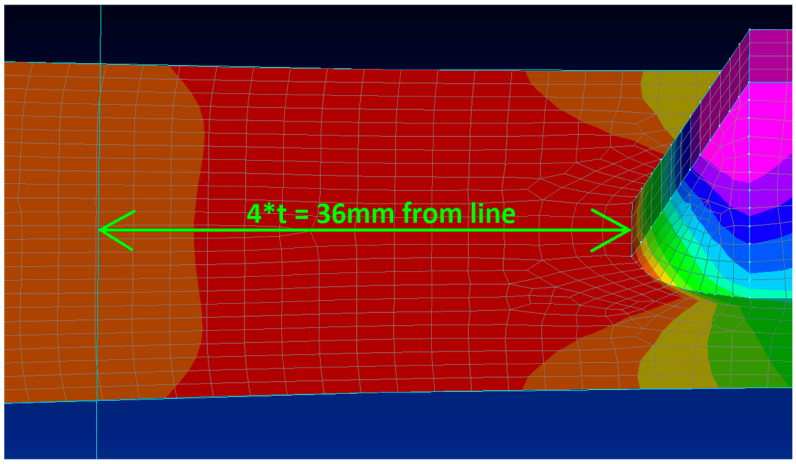

Figure 4. Installation location of resistance strain gauge.

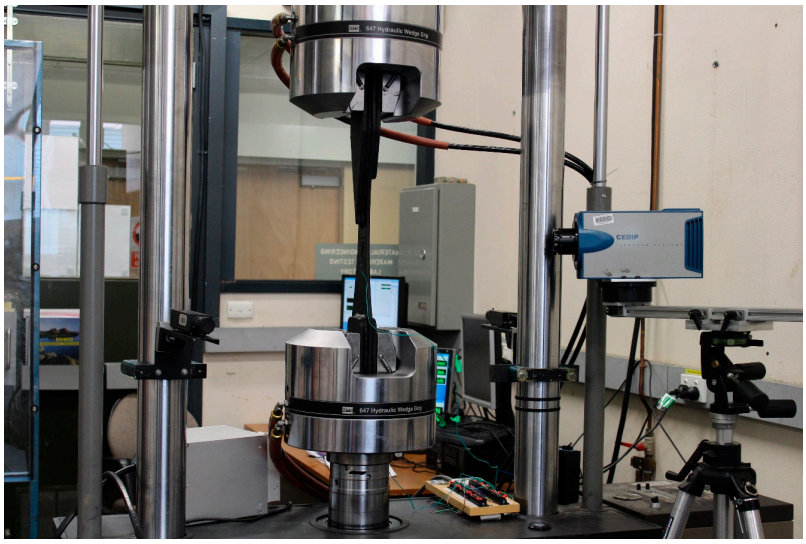

Figure 5. Initial specimen and specimen in the test machine.

A CEDIP (Paris, France) JADE medium-wave infrared camera was then used to obtain the stress distribution of the welded specimen under cyclic loading. The CEDIP JADE medium-wave infrared camera has three output modes. The E mode is the stress difference output mode. Just select this output mode to obtain sigma thermal values. The equipment for strain and thermal stress measurement is shown in Figure 5. A 12.5 mm lens Sony

(Tokyo, Japan) digital camera (25FM25L TAMRON) was used to detect the cracks; see Figure 6. The standard lens plus a 5~10 mm extension ring was used. The infrared camera system and digital camera were used to monitor the crack growth from the initiation of the crack to the failure of the specimen. The maximum strain measurement results of the toe side and blunt side at 36 mm from the hot spot were 1276 ± 20 $\mu\varepsilon$ and 624 ± 20 $\mu\varepsilon$, respectively. Their converted stresses were 255.2 ± 4 MPa and 124.7 ± 4 MPa, respectively. The infrared measurement results of $\Delta\sigma$ at these corresponding positions were 234.7 MPa and 113.6 MPa. Since the stress ratio $R = \frac{\sigma_{min}}{\sigma_{max}} = \frac{5}{75} = 0.067$ was used in the test, the infrared measurement results of the maximum stress (σ_{max}) on the toe side and blunt side were 251.6 MPa and 121.8 MPa. In addition, the infrared measurement result of $\Delta\sigma$ and its converted result of σ_{max} at the toe root of the specimen were 470.5 and 504.3 MPa, respectively. Here, σ_{max} and σ_{min} are the maximum and minimum stresses on the surface of the centre sill at 36 mm from the toe under cyclic stress, respectively. It can be seen that the resistance strain and infrared measurement results are very close to the finite element analysis results. This ensures that the test results are as consistent as possible with the actual loading conditions of the centre sill.

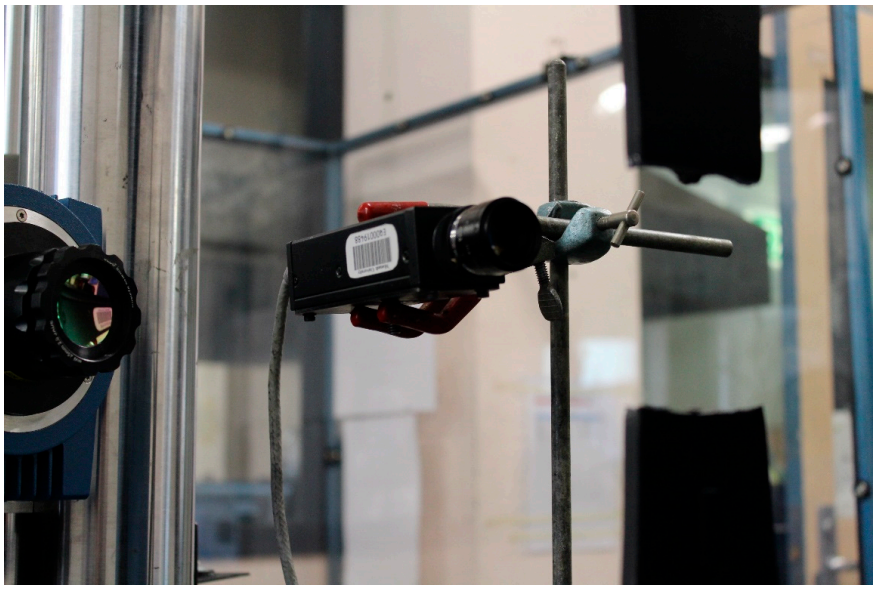

Figure 6. A 12.5 mm lens Sony digital camera with 5~10 mm extension.

The crack length was measured by using a digital camera equipped with a microscope lens as the main method and infrared observation as the auxiliary method. The crack tip can be easily found by using the characteristics of the main stress and the distribution of the infrared detected on the line perpendicular to the loading direction at the front of the crack tip and with a double peak shape and opposite stress phase. If the position of the crack initiation were known, the digital camera equipment could be focused onto the area to assist with a better diagnosis of crack propagation. At 437,500 cycles, one crack was initiated. After 762,500 cycles, the crack grew rapidly until failure. Total failure occurred at 762,701 cycles. The stress field (E model) of the specimen viz. the number of cycles is shown in Figure 7.

Figure 8 shows the cross-section after fracture. It can be clearly seen that the process of crack growth from its initial length up to the critical crack length can be represented as three phases: phase I, phase II and phase III, respectively. Phase I: The crack originates from both sides of the toe. Phase II: Under the cyclic loading, two small surface cracks continue to grow until they merge into a large semi-elliptical surface crack. Phase III: In this phase, the crack penetrates the surface to form a complex 2D crack.

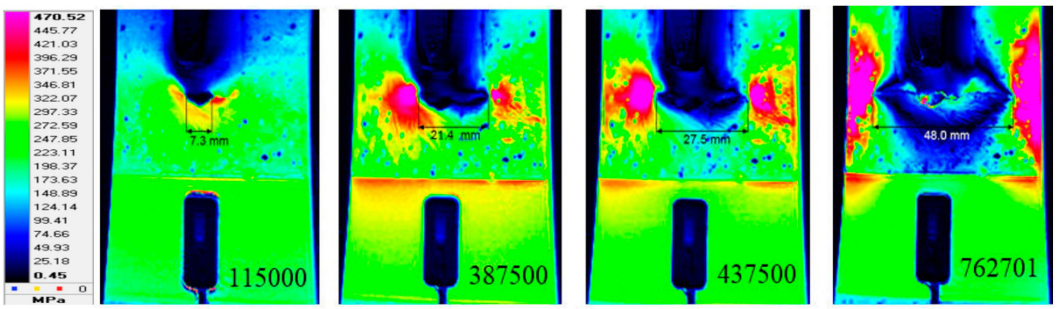

Figure 7. Stress field (E model) of specimen viz. number of cycles. Stress units are in Pa.

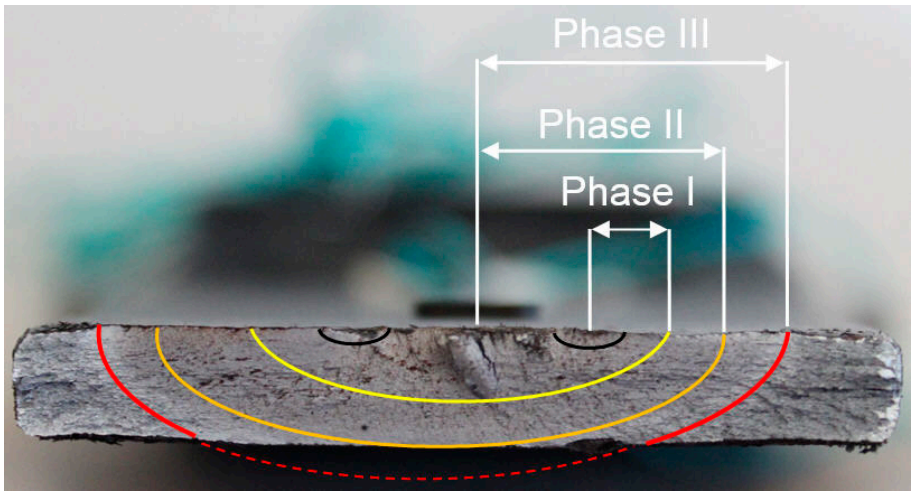

Figure 8. Cross-section after fracture.

4. Crack Growth Analysis and Results

The purpose of this section is to present the results of the crack growth analysis of the specimen for comparison with the test results. The analysis has two parts. At each stage in the analysis, i.e., for each crack shape, the computational methodology presented in [13,14] is (first) used to determine the stress intensity factors. Having thus determined the stress intensity factor solution around the crack front the Hartman–Schijve variant of the Nasgro equation [23] is then used used to describe the increment in crack growth. This particular variant of the Nasgro crack growth equation takes the form:

$$\frac{da}{dN} = D\left[\frac{\Delta K - \Delta K_{thr}}{\sqrt{1-\frac{K_{max}}{A}}}\right]^{p} \quad (1)$$

Here ΔK_{thr} is defined as an apparent fatigue threshold and A is the cyclic fracture toughness. D and p are material constants, which are measured experimentally, ΔK and K_{max} are the range of stress intensity factor and maximum stress intensity factor in a load cycle, respectively. The above analysis method can be simply summarised as follows:

- Finite element analysis was performed on the unruptured (uncracked) structure;
- Fatigue critical locations and the stresses on potential crack surfaces were found (note that the stresses extracted here are the concentrated area directly near the toe and not at the strain gauge location);
- The stress intensity factor solution K(a, c) around the crack was calculated as outlined in [13]. Here "a" was the crack depth and "c" was the surface crack length, respectively;
- The increment in the crack length and the crack depth for a given load cycle is then calculated using the Hartman–Schijve variant of NASGRO crack growth equation and the stress intensity factor solution determined above.

It is worth noting that this technique is computationally and analytically efficient. Only one finite element stress analysis is required for the uncracked structure. Furthermore, since the crack is not explicitly modelled, it is not necessary to use a fine mesh at the crack tip to reflect its singularity. This greatly shortens the analysis time. This method has been successfully used to solve fatigue analysis problems for various complex cracked structures [31,32]. Therefore, it should be a viable approach for the crack growth analysis of hopper wagons.

Due to the geometry and load symmetry of the specimen, only half of it needs to be analysed. The geometry and mesh used for the finite element analysis are provided in Figure 9. The maximum principal stress at the toe and the blunt side are shown in Figure 10. It was thought that surface roughness/irregularities may have an effect on the stresses at the critical region and hence on the resultant stress intensity factors. A local stress factor given by $K_t = \sigma_{Thermal}/\sigma_{FEM}$ was used to account for local stress concentration due to surface roughness/irregularities on the welded surface. $\sigma_{Thermal}$ is the stress obtained by infrared measurement of the specimen during the test, and σ_{FEM} is the result obtained by finite element analysis. (Here, it is assumed that the surface of the specimen is smooth. However, the surface of the actual specimen was rough due to corrosion.)

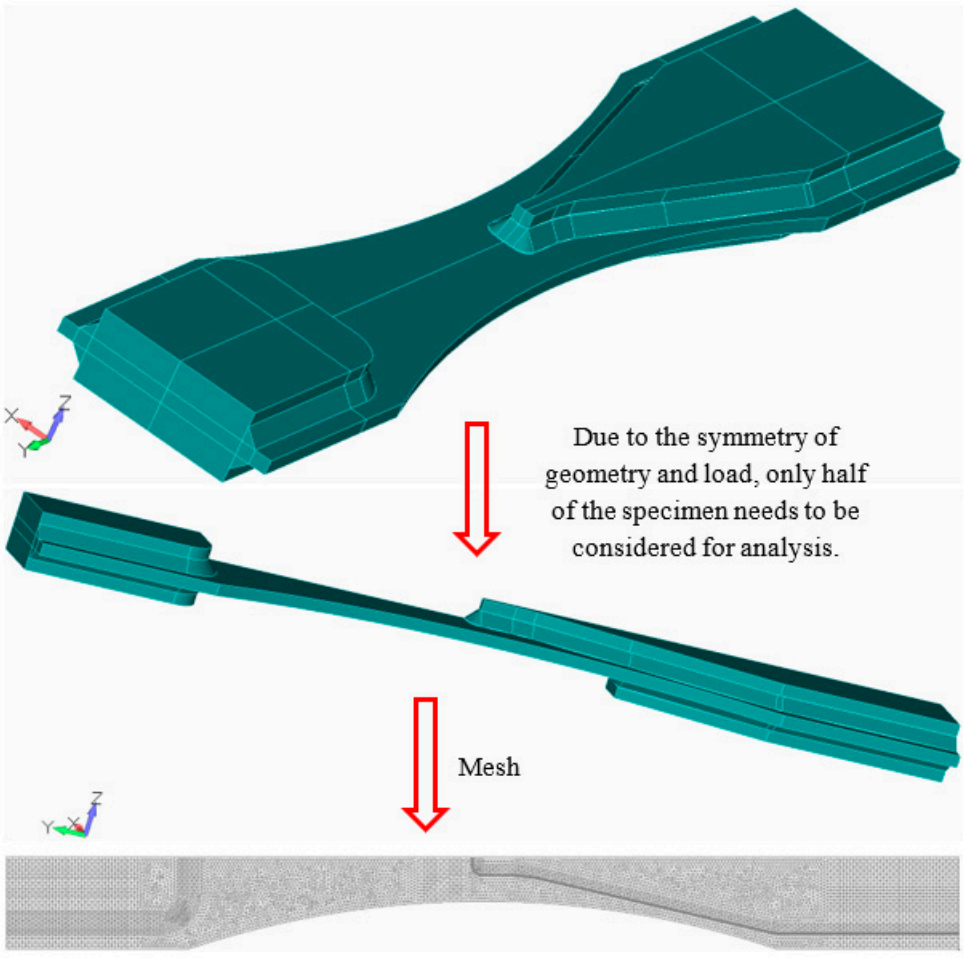

Figure 9. The geometry of the specimen and the mesh for finite element analysis.

In the crack growth analysis, the material was assumed to be a mild steel with yield strength = 379 MPa and ultimate tensile strength = 552 MPa, respectively. Here, the change in the stress intensity factor and crack growth rate are expressed in MPa and m/cycle, respectively. The threshold was assumed to be 0 MPa. The constants used in the crack growth equation were $D = 3.5 \times 10^{-10}$ (m/cycle) and $p = 2.0$, together with 'A' of 54.4 MPa$\sqrt{}$m.

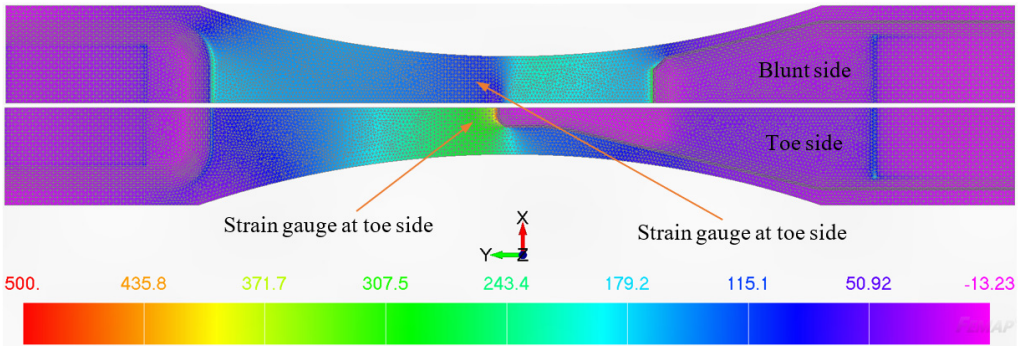

Figure 10. Maximum principal stress at both toe and blunt side of welded specimen, The stress units are in MPa.

The crack growth process in the specimen can be analysed by means of three phases: phase I, phase II and phase III, respectively (see Figure 11). It is worth noting that, in phase I, the two cracks initiated from the two sides of the toe had an interaction effect on the growth process. The influence factor was considered in the calculation of stress intensity factor [32]. The analysis results shown that, in phase I and phase II, the predicted results were quite consistent with the test results. In phase III, there was a certain difference between the predicted and the tested results, resulting in an estimated life that was 4.8% shorter than the test results. However, it was still within an acceptable range. The main reason is that the crack in the third phase had a strange shape, and there was no accurate solution for the stress intensity factor. In this phase, a simple method [3,32] was used to calculate the stress intensity factor, which results in a more conservative solution. It should be stressed that the residual stress in the welded specimen was not included in this analysis. Since the welded specimen was subjected to Ultrasonic Impact Treatment (UIT), the effect of the residual stress at the weld toe on the crack growth was neglected. It is worth noting that at the beginning of phase II, since the two small cracks have grown into a large surface crack, the crack centre has suddenly moved from the crack centre of each small crack to the symmetric centre of the two cracks. At this time, the crack length has a sudden change (suddenly becomes longer). The vertical part of the red curve at the beginning of phase II in Figure 11 reflects this sudden change in crack length.

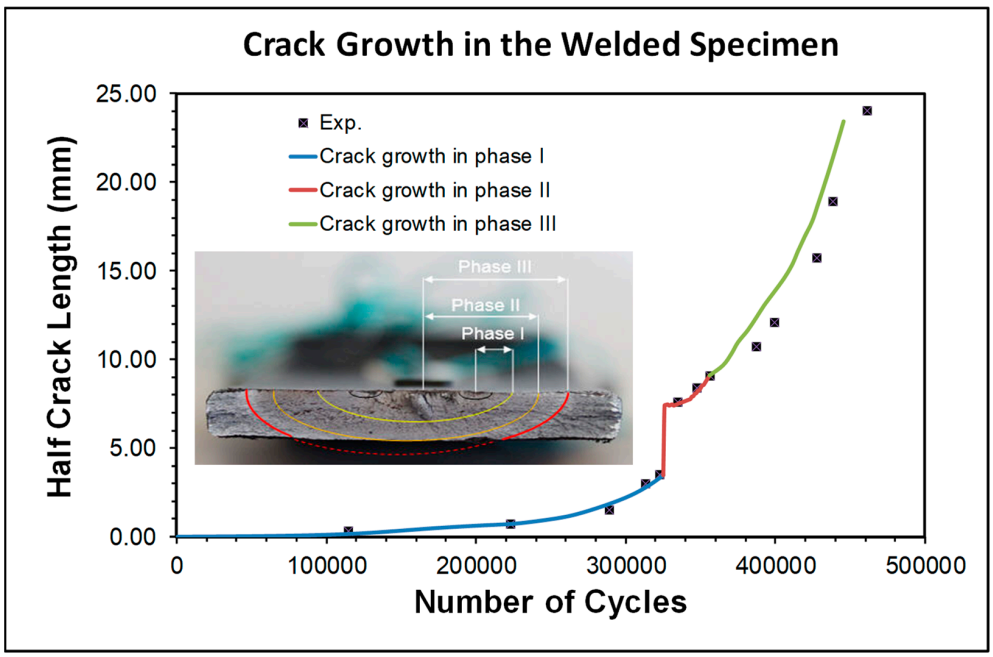

Figure 11. Comparison of measured and computed crack growth histories for welded specimen.

5. Conclusions

This paper used materials cut directly from a centre sill to make the specimen. The real welded toe structure that will suffer fatigue damage is retained in the specimen. The maximum traction loads transmitted to the centre sill during the operation of the hopper wagon were used as the test's load. This paper has also shown how, by combining strain gauges, infrared thermography, the three-dimensional finite element alternating technique and the Hartman-Schijve crack growth equation, with the fatigue threshold set to a small near-zero value, it is possible to accurately compute the crack growth history in a component that is representative of a critical member in a hopper wagon.

As such, this paper extends the methodology used to assess the durability of aerospace structures to welds in rail structures.

Author Contributions: Conceptualisation—R.J. and D.P.; Formal analysis—D.P.; Methodology—R.J. and D.P.; Writing—original draft—D.P.; Writing—review and editing—A.S.M.A.; Project administration—R.J. All authors have read and agreed to the published version of the manuscript.

Funding: This research received no external funding.

Institutional Review Board Statement: Not Applicable.

Informed Consent Statement: Not Applicable.

Data Availability Statement: The data presented in this study is available in the manuscript. For further enquiries, please contact with Corresponding author.

Acknowledgments: The authors would like to thank Ken Cairns for his assistance in the fatigue testing.

Conflicts of Interest: The authors declare no conflicts of interest.

References

1. Richmond, S.; Millsteed, W.; Wilson, R.; Prospects for Iron Ore, Steel and Nickel. Abare. 2006. Available online: https://search.informit.org/doi/abs/10.3316/informit.080674486571037 (accessed on 5 October 2024).
2. Auslink, G.P. Towards the national Land Transport Plan, Department of Transport and Regional Services. 2002. Available online: https://www.vgls.vic.gov.au/client/en_AU/vgls/search/detailnonmodal/ent:$002f$002fSD_ILS$002f0$002fSD_ILS:307473/ada?qu=Road+construction+planning.&d=ent://SD_ILS/0/SD_ILS:307473~ILS~24&ic=true&ps=300&st=PD&h=8 (accessed on 5 October 2024).
3. Peng, D.; Jones, R.; Hui, D. An engineering approach to the fracture assessment of hopper wagons. *Eng. Fract. Mech.* **2017**, *179*, 79–92. [CrossRef]
4. Suprianto, T.; Syaifudin, A.; Pamungkas, L.W.; Ariatedja, J.B.; Farid, A.R. Effect of Fluctuating Load on Fatigue of PPCW Flat Wagon. *Int. J. Mech. Eng. Sci.* **2023**, *7*, 26–35. [CrossRef]
5. Vega, B.; Pérez, J.A. Comparative analysis of fatigue strength of a freight wagon frame. *Weld. World* **2024**, *68*, 321–332. [CrossRef]
6. Fernández, J.Á.P. Theoretical and Experimental Study of the Fatigue Behaviour of Large Passenger Transport Vehicles under Dynamic Operating Loads. Ph.D. Thesis, Universidad Politécnica de Madrid, Madrid, Spain, 2017. Available online: https://oa.upm.es/47667/ (accessed on 5 October 2024).
7. Slavchev, S.; Maznichki, V.; Stoilov, V.; Enev, S.; Purgic, S. Comparative Analysis of Fatigue Strength of an Y25LS-K Bogie Frame by Methods of UIC and DVS 1612. Czech Republic, 2018. Available online: https://www.researchgate.net/publication/337334934_COMPARATIVE_ANALYSIS_OF_FATIGUE_STRENGTH_OF_AN_Y25LS-K_BOGIE_FRAME_BY_METHODS_OF_UIC_AND_DVS_1612 (accessed on 5 October 2024).
8. Stoilov, V.; Slavchev, S.; Purgic, S. *Study of Fatigue in Welded Joints and Stress Notches of Wagon*; Technical University of Sofia, Faculty of Transport: Sofía, Bulgaria, 2014.
9. DVS, Technical Comittee, Working Group. 'Welding in Railway Vehicle Manufacturing'. Technical Code DVS 1612. Design and Endurance Strength Analysis of Steel Welded Joints in Railvehicle Construction. DVS—German Welding Society. 2014. Available online: https://www.dvs-regelwerk.de/en/guidelines-nodes/guideline-dvs-1612-08-2014 (accessed on 5 October 2024).
10. ERRI. ERRI B 12/RP 60—2nd Edition. Tests to Demonstrate the Strength of Railway Vehicles. Regulations for Proof Tests Andmaximum Permissible Stresses. ERRI (European Rail Research Institute), 2001. Available online: https://shop.uic.org/en/b-12-wagons/5888-regulations-for-proof-tests-and-maximum-permissible-stresses-2nd-edition.html (accessed on 5 October 2024).
11. UIC. UIC B 12/RP 17 9th Edition. WAGONS. Programme of Tests to be Carried out on Wagons with Steel Under Frame and Body Structure (Suitable for Being Fitted with the Automatic Buffing and Draw Coupler) and on Their Cast Steel Frame Bogies. UIC (International Union of Railways), 2012. Available online: https://shop.uic.org/en/b-12-wagons/5839-wagons-programme-of-tests-to-be-carried-out-on-wagons-with-steel-underframe-and-body-structure-suitable-for-being-fitted-with-the-automatic-buffing-and-draw-coupler-and-on-their-cast-steel-frame-bogies.html (accessed on 5 October 2024).

12. *FEMAP—Finite Element Modelling and Post Processing @Version 11.4.1, 5800 Granite Pkwy #600*; Siemens Industry Software Inc.: Plano, TX, USA, 2019; Available online: https://www.plm.automation.siemens.com/media/global/en/Siemens-SW-Simcenter-Femap-version-2022-1-1-FS-84339-D3_tcm27-104025.pdf (accessed on 5 October 2024).
13. Jones, R.; Peng, D.; Pitt, S.; Wallbrink, C. Weight Functions, CTOD, and Related Solutions for Cracks at Notches. *Eng. Fail. Anal.* **2004**, *11*, 79–114. [CrossRef]
14. Peng, D.; Huang, P.; Jones, R. Practical computational fracture mechanics for aircraft structural integrity. In *Aircraft Sustainment and Repair*; Butterworth-Heinemann Press: Oxford, UK, 2018; Chapter 4; pp. 67–128. ISBN 978008100548.
15. Main, B.; Evans, R.; Walker, K.; Yu, X.; Molent, L. Lessons from a Fatigue Prediction Challenge for an Aircraft Wing Shear Tie Post. *Int. J. Fatigue* **2019**, *123*, 53–65. [CrossRef]
16. Tan, J.L.; Chen, B.K. Coalescence and growth of two coplanar short cracks in AA7050-T7451 aluminium alloys. *Eng. Fract. Mech.* **2013**, *102*, 324–333. [CrossRef]
17. Tan, J.L.; Chen, B.K. A new fracture area method for predicting the growth of a newly coalesced crack in AA7050-T7451 aluminium alloy. *Theor. Appl. Fract. Mech.* **2015**, *75*, 146–150. [CrossRef]
18. Tan, J.L.; Chen, B.K. Prediction of fatigue life in aluminum alloy (AA7050-T7451) structures in the presence of multiple artificial short cracks. *Theor. Appl. Fract. Mech.* **2015**, *78*, 1–7. [CrossRef]
19. Pipkins, S.D.; Atluri, S.N. Applications of the three dimensional method finite element alternating method. *Finite Elem. Anal. Des.* **1996**, *23*, 133–153. [CrossRef]
20. Pitt, S.; Jones, R.; Atluri, S.N. Further studies into interacting 3D cracks. *Comput. Struct.* **1999**, *70*, 583–597. [CrossRef]
21. Nishioka, T.; Atluri, S.N. Analytical solution for embedded elliptical cracks, and finite element alternating method for elliptical surface cracks, subjected to arbitrary loadings. *Eng. Fract. Mech.* **1983**, *17*, 247–268. [CrossRef]
22. Simon, H.L.; O'Donoghue PEAtluri, S.N. A finite-element-alternating technique for evaluating mixed modes stress intensity factors for part-elliptical surface flaws. *Int. J. Numer. Methods Eng.* **1987**, *24*, 689–709. [CrossRef]
23. Park, J.H. A Review on Finite Element Alternating Methods for Analyzing 2D and 3D Cracks. *Digit. Eng. Digit. Twin* **2024**, *2*, 79–101. [CrossRef]
24. Jones, R. Fatigue Crack Growth and Damage Tolerance. *Fatigue Fract. Eng. Mater. Struct.* **2014**, *37*, 463–483. [CrossRef]
25. Shamir, M.; Zhang, X.; Syed, A.K. Characterising and representing small crack growth in an additive manufactured titanium alloy. *Eng. Fract. Mech.* **2021**, *253*, 107876. [CrossRef]
26. Dastgerdi, J.N.; Jaberi, O.; Remes, H.; Lehto, P.; Toudeshky, H.H.; Kuva, J. Fatigue damage process of additively manufactured 316L steel using X-ray computed tomography imaging. *Addit. Manuf.* **2023**, *70*, 103559. [CrossRef]
27. Han, S.; Dung Dinh, T.; De Baere, I.; Boone, M.; Josipovic, I.; Van Paepegem, W. Study of the effect of defects on fatigue life prediction of additive manufactured Ti-6Al-4V by combined use of micro-computed tomography and fracture-mechanics-based simulation. *Int. J. Fatigue* **2023**, *180*, 108110. [CrossRef]
28. Ye, J.; Syed, A.K.; Zhang, X.; Eimer, E.; Williams, S. Fatigue crack growth behaviour in an aluminium alloy Al-Mg-0.3Sc produced by wire based directed energy deposition process. *Fatigue Fract. Eng. Mater. Struct.* **2023**, *46*, 3927–3938. [CrossRef]
29. Shamir, M.; Zhang, X.; Syed, A.K.; Sadler, W. Predicting the Effect of Surface Waviness on Fatigue Life of a Wire Arc Additive Manufactured Ti-6Al-4V Alloy. *Materials* **2023**, *16*, 5355. [CrossRef]
30. Markham, M.J.; Fatemi, A.; Phan, N. Mixed-Mode Small Fatigue Crack Growth Rates and Modelling in Additively Manufactured Metals. *Int. J. Fatigue* **2024**, *183*, 108258. [CrossRef]
31. Peng, D.; Jones, R.; Constable, T.; Lingamanaik, S.N.; Chen, B.K. The tool for assessing the damage tolerance of railway wheel under service conditions. *Theor. Appl. Fract. Mech.* **2012**, *57*, 1–13. [CrossRef]
32. Peng, D.; Jones, R.; Constable, T. Tools and methods for addressing the durability of rolling stock. *Eng. Fail Anal.* **2013**, *34*, 278–289. [CrossRef]